Preferred citation: M. Kataja and P. Hirsilä. Application of Ultrasound Anemometry for Measuring Filtration of Fibre Suspension. In **The science of papermaking**, *Trans. of the XIIth Fund. Res. Symp. Oxford, 2001*, (C.F. Baker, ed.), pp 591–604, FRC, Manchester, 2018. DOI: 10.15376/frc.2001.1.591.

APPLICATION OF ULTRASOUND ANEMOMETRY FOR MEASURING FILTRATION OF FIBRE SUSPENSION

Markku Kataja[1,2] *and Pekka Hirsilä*[2]

[1]University of Jyväskylä, Department of Physics,
P.O. Box 35, FIN-40351 Jyväskylä, Finland
[2]VTT Energy, Technical Research Centre of Finland,
P.O. Box 1603, FIN-40101 Jyväskylä, Finland

ABSTRACT

We introduce a novel method for measuring the properties of consolidating wood fibre network during filtration of liquid-fibre suspension. The device consists of a hand-sheet mould equipped with a pulsed ultrasound-Doppler anemometer for measuring the local time-dependent velocity field of the fibre phase during vertical filtration. Simultaneously, the total flux of the suspension and fluid pressure loss through the filtrated fibre layer are measured. Based on this experimental information other relevant flow quantities can be computed. We thus find the space-time evolution of velocity, volume fraction and pressure (stress) fields separately for the fluid phase and for the fibre phase. This method allows us to experimentally study the details of the consolidation process in dynamic conditions. The device can be applied as an advanced laboratory test instrument for measuring relevant physical fibre network properties. As a result we present, e.g., the measured local stress-strain history of the consolidating fibre layer during a filtration experiment.

1 INTRODUCTION

As an essential process of paper forming [1–5], filtration of wood fibres has been studied in laboratory conditions, e.g., by measuring fluid flux and pressure loss through the consolidating fibre layer in a hand-sheet mould or in various dynamic filtration devices [6–9]. Such studies mostly address bulk properties of the filtrate such as flow resistance and the average degree of consolidation. Instead, they do not give much information on the detailed dynamics of the filtration process itself or on the evolution of the local conditions inside the filtered layer such as density distribution, flow resistance distribution and stress state of the forming fibre network. Such an experimental information would however be invaluable, e.g., for analysis and realistic modelling of paper-making processes involving filtration and consolidation of fibres.

In this paper we introduce a novel method for measuring the local velocity field of fibres during filtration of dilute liquid-fibre suspension. The device consists of a simple gravity driven hand-sheet mould equipped with a pulsed ultrasound-Doppler anemometer for measuring the local time-dependent velocity field of the fibre phase during vertical filtration. The total flux of the suspension is independently measured using a separate ultrasound transducer to detect the position of the free surface of the suspension in the mould. Pressure loss caused by the consolidating fibre layer is measured by a pressure sensor located under the filtration wire. Using the two-phase flow equations appropriate for the present system, the other relevant flow quantities (fields) such as fluid velocity and pressure, consistency, flow resistance and structural stress of the fibre network can be computed based on the measured data. The method can thus provide detailed information on the dynamics of filtration and material properties of the consolidating fibre layer that has not been previously available.

2 FILTRATION EQUATIONS

Before discussing the experimental set-up in more detail, we briefly review the theoretical background of two-phase flow that will comprise the starting-point for our data analysis at a later stage.

We thus consider a suspension that contains a continuous fluid phase ("free water") and a particulate solid phase that consists of wet fibres, i.e., of dry fibres and the water bound by the absorbent fibre material ("bound water"). A vertical (z-directional) time dependent flow and filtration of such a suspension is governed by the following continuity and momentum Equations (10, 11).

$$\frac{\partial}{\partial t}\phi_f + \frac{\partial}{\partial z}(\phi_f \tilde{u}_f) = 0 \tag{1}$$

$$\frac{\partial}{\partial t}\phi_s + \frac{\partial}{\partial z}(\phi_s \tilde{u}_s) = 0 \tag{2}$$

$$\phi_f \frac{\partial}{\partial z}\tilde{p}_f = D - \phi_f \tilde{\rho}_f g \tag{3}$$

$$\phi_f \frac{\partial}{\partial z}p_s = -D - \phi_f \phi_s (\tilde{\rho}_s - \tilde{\rho}_f) g. \tag{4}$$

Here, subscripts *f* and *s* refer to the fluid phase and the solid phase, respectively, ϕ_a is the volume fraction, $\tilde{u}_a$ is the flow velocity in *z*-direction, p_a is the pressure, $\tilde{\rho}_a$ is the density for phase $a = f,s$, D is the momentum transfer term between phases and g is the acceleration due to gravity. The notation $\tilde{x}_a$ denotes an intrinsic average of quantity x_a, i.e., an average taken over the volume ΔV_a occupied by phase a in a general averaging volume ΔV (such that $\phi_a = \Delta V_a / \Delta V$). Notice that the fluid pressure $\tilde{p}_f$ is defined as an intrinsic average (often termed as "pore pressure"), whereas the solid pressure p_s, or more exactly, the normal structural stress in *z*-direction, is defined as a partial average, i.e., an average taken over the total averaging volume ΔV [10]. Notice also, that the solid pressure that appears in Equation (4) does not include the stress induced in solid particles by the pressure of surrounding fluid, but only the effective stress that arises due to interfibre contacts and deformation of the fibre matrix [12–14]. For the flow conditions prevailing in the filtration experiment Terzaghis principle [15] is applicable, and the total pressure of the suspension is given by $p_T = p_s + \tilde{p}_f$ [13].

Equations (1–4) can be derived in a straightfoward manner from the more general flow equations of two-phase flow with no mass transfer between phases ignoring inertial, viscous and turbulent terms. Adding the continuity Equations (1) and (2) and using the identity $\phi_f + \phi_s = 1$ gives

$$\frac{\partial}{\partial z}q_T = 0, \tag{5}$$

where

$$q_T = \phi_f \tilde{u}_f + \phi_s \tilde{u}_s \tag{6}$$

is the total flux of the suspension. According to Equation (5) the total flux

does not depend on the spatial coordinate z, and $q_T = q_T(t)$. Similarly, adding the momentum Equations (3) and (4) leads

$$\frac{\partial}{\partial z} p_T = -\rho g, \tag{7}$$

where $\rho = \phi_f \tilde{\rho}_f + \phi_s \tilde{\rho}_s$ is the density of the suspension.

3 EXPERIMENTAL SET-UP

An overview of the filtration device used in the present experiments is shown in Figure 1. The device consists of a sealed tank and a riser tube of diameter 160 mm with a plastic wire and a wire support grid. Fluid can be driven up and down in the riser tube by adjusting air pressure in the tank. The fluid

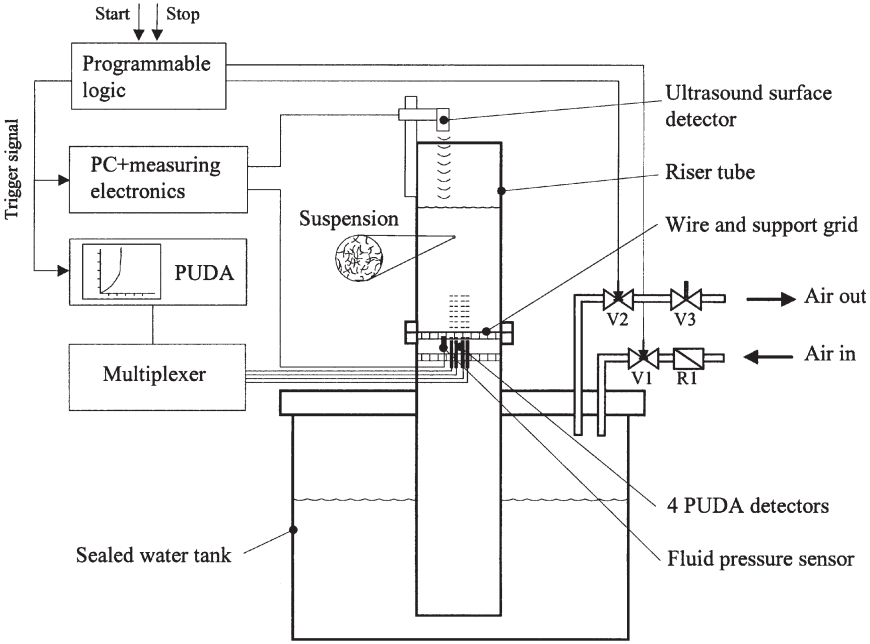

Figure 1 Schematic illustration of the filtration device.

motion and the measuring procedure is controlled by a programmable logic unit.

The vertical velocity of fibres is measured through the wire by a commercial pulsed ultrasound-Doppler anemometer (PUDA) (DOP 1000-device by Signal-Processing S.A., Lausanne, Switzerland). Four ultrasonic probes of diameter 5 mm are assembled in upright position symmetrically around the centerline of the riser tube and about 10 mm below the wire. The probes are connected to PUDA through a multiplexer. Within the set-up used in the present experiments, the probes can detect the local vertical velocity of fibres through the wire and up to the distance of approximately 70 mm above the wire. The spatial resolution is approximately 0.3 mm in the z-direction. The measuring frequency is selected such that the time for measuring one profile with a single probe is about 56 ms. In order to reduce the effects of local velocity fluctuations of the suspension and of noise inherent in the PUDA measurement, the final fibre velocity profile at each instant of time is defined as the average of the four consecutive profiles measured with the four probes. More than 130 such velocity profiles are recorded during a typical total filtration time of 30 seconds. Prior to analysis, the velocity data is appropriately filtered in order to remove the residual spurious noise. As a result, we thus get the experimental vertical velocity field $\tilde{u}_s = \tilde{u}_s(t,z)$ (see previous section) during the filtration process in a layer that ranges from the surface of the wire about 70 mm upwards near the center of the wire.

The instantaneous location of the free surface of the fibre suspension in the riser tube is detected by an ultrasound position sensor. Differentiating the surface position data with respect to time gives the surface velocity that equals the total flux $q_T = q_T(t)$ of the suspension.

Fluid pressure at the wire is measured by a pressure detector placed immediately under the wire. The offset value of the sensor is adjusted such that the reading corresponds to fluid pressure at the upper surface of the wire. Notice that inertial effects on the measured fluid pressure can be neglected due to the relatively low filtration velocity. In test runs carried out with pure water it was observed that the pressure loss caused by the wire is also negligible.

The measurement is initiated by filling the tank by distilled water at room temperature. Water is compelled in the riser tube by opening valve V1. The desired filling level is determined by an adjustable pressure regulator R1. The possible air entrapped in and below the wire is removed manually using a suction tube. A weighed amount of fibres is then carefully mixed in the riser tube. After mixing, suspension is allowed to settle for a few seconds. During this time water level in the tube is slowly rised in order to compensate free sedimentation thus preventing premature accumulation of fibres on the

surface of the wire. The measurement is started by a push-button signal given to the programmable logic unit which then triggers all the measurements simultaneously and slowly opens valve V2. The flow rate during filtration can be reduced by adjusting valve V3. Otherwise, flow is driven by gravity. The measurement is completed by closing valve V2 in order to stop the flow, and saving the collected data for later analysis. The flow is usually stopped well before the fluid surface in the raiser tube reaches the filtrated fibre layer thereby preventing air from entering the suspension and the wire. The experiment can thus be repeated for a number of times using the same sample of fibres by raising the fluid level and remixing the fibres.

With the used PUDA device, the velocity resolution is given by $v_{max}/128$, where v_{max} is the maximum measurable velocity that can be adjusted in a large range by the device parameters. Measuring the slow residual motion of the filtrated fibre network on top of the wire requires quite high velocity resolution, and limits the maximum velocity available. Here, we have selected $v_{max} \cong 22$ mm/s. In order to allow for the possible velocity fluctuations of the locally inhomogeneous solid phase to be correctly recorded, the actual maximum average flow velocity in the experiment is limited to be of the order of 10 mm/s.

4 DATA ANALYSIS AND RESULTS

The data analysis of the filtration experiment is based on Equations (1) through (4) with an assumption that the solid velocity field $\tilde{u}_s(t,z)$ is given by the experiment in the entire flow region above the wire. The experimental procedure described above provides us the measured solid velocity field $\tilde{u}_s(t,z)$ in the PUDA measurement range (i.e., in the layer of thickness ~70 mm just above the wire). The amount of fibres used in the present experiments is selected such that marked consolidation of fibre network takes place well in the PUDA measurement range. Above the filtration region the suspension is in a state of free sedimentation where the structural stress of the fibre network is negligible and all velocities are independent of the distance z from the wire. This is also clearly seen in the instantaneous solid velocity profiles measured by PUDA at any given time as the measured velocity approaches a constant value towards the maximum measurable distance. We thus conclude that it is appropriate to extrapolate this limiting value into the entire flow region above the PUDA measuring range.

Using the measured solid velocity field $\tilde{u}_s(t,z)$ we can readily solve the solid phase pathlines $z_s(t)$ in the t-z-plane using the equation

$$\frac{dz_s}{dt} = \tilde{u}_s(t,z_s). \tag{8}$$

The solid volume fraction ϕ_s is proportional to the mass consistency of dry fibres C_m (see Equation (12) below). Writing the solid phase continuity Equation (2) in terms of C_m, and applying it along a pathline determined by Equation (8) yields

$$\frac{dC_m}{dt} = C_m \frac{\partial}{\partial z} \tilde{u}_s\,(t,z_s), \tag{9}$$

where the derivative with respect to time denotes the convective derivative along solid pathlines. Given the initial consistency $C_{m0}(z)$, we can thus solve the dry fibre consistency $C_m(t,z)$ in the entire flow region.

In what follows it will be assumed that the initial consistency C_{m0} is constant. Notice that in analysing the experimental data using the one-dimensional time-dependent model, all the flow quantities are understood to represent an average of the corresponding quantity over the cross-section of the riser tube. Indeed, spatial averaging is present in the measured PUDA data due to the physical size of the transducers, the use of multiple probes and filtering of data. Owing to the simple measuring method used, the experimental values of the total flux also represent such an average. Consequently, the local fluctuations caused by the underlying floc structure of the fibre network are strongly quenched in the measured data, and ignored in the present analysis.

The new method was first applied in a suspension made of unbeaten bleached softwood fibres mixed in water with an initial consistency $C_{m0} \approx 0.2\%$. An example of typical measured solid phase pathlines in the t-z-plane are shown in Figure 2a) together with the measured position of the free surface. A more detailed flow pattern in the filtration zone near the wire is shown in Figure 2b) together with contours of constant C_m as solved using Equation (9).

In the free sedimentation region well above the filtration region, the solid pathlines are nearly parallel to each other. At this region, consistency C_m is constant and equals the initial consistency. The upper thick line indicates measured position of the surface. Sedimentation is visible as increasing distance between the surface line and the uppermost solid pathline. At the end of experiment, $t = 30$ s, the distance between the two lines is approximately 25 mm which corresponds the visually observed thickness of the clear water layer next to the surface.

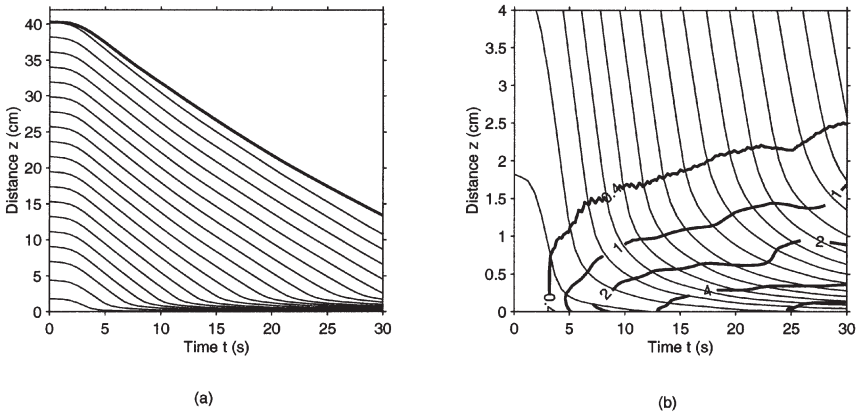

Figure 2 **a)** Measured solid pathlines in t-z-plane in the riser tube. The uppermost thick line shows the location of the fluid surface as measured by ultrasound surface detector. The wire is located at $z = 0$. **b)** Solid pathlines (thin lines) and contours of constant consistency (thick lines) near the wire. Labelling indicates consistency in (%).

The filtration region near the wire is indicated by the marked bending of pathlines towards horizontal as the solid velocity $\tilde{u}_s$ approaches zero (and the fluid velocity $\tilde{u}_f$ slightly increases). The consistency increases as the fibre network is compressed against the wire by the fluid flow. As shown by Figure 2b), the slowing down of the solid phase starts approximately at a consistency of 0.4%, which indeed is near the theoretical sedimentation consistency of the present fibres, i.e., the consistency in which the fibres have enough contacts such that the network can carry structural stress [16]. The data does not however show any clear boundary between the filtrated layer and the free sedimentation layer.

In order to extract more information on the detailed filtration mechanism and on the relevant material properties of the fibre network during filtration, it is instructive to study the evolution of various flow quantities along the pathlines of the solid phase. In particular, the experimental data as shown in Figure 2 allows us to follow the evolution of consistency, velocity and even the stress state of a given fibre layer during filtration.

Figure 3a) shows the consistency C_m as a function of time along a subset of pathlines shown in Figure 2. Each curve in Figure 3a) thus represents the evolution of the density of various fibre layers during filtration. At early times the consistency of a given fibre layer is constant and equals the initial

consistency. As the layer enters the filtration region, the consistency starts to increase – the later, the higher is its initial position in the riser tube. For all pathlines, the increase seems continuous and smooth. At least in the present experiment where unbeaten fibres are used and the flow is relatively slow as compared, e.g., with filtration speed typically found in forming of paper, the process thus appears as a gradual continuous precipitation rather than a clear-cut filtration with well separated free suspension and filtrated layer.

Similarly to Figure 3a), one can also find the evolution of the velocity of each fibre layer during the process. In Figure 3b) is shown the relative velocity $\tilde{u}_s/q_T$ as a function of consistency C_m along the same pathlines that were used in Figure 3a). Remarkably, the data for all the pathlines now collapses approximately on a same curve indicating strong correlation between the two quantities. In the present experiments the evolution of all the layers thus appears similar in the sense that the relative velocity of the layer only depends on the density it has reached, and not explicitly on time. It remains to be seen whether such a scaling law is valid more generally.

We now turn to the interesting problem of material properties of the fibre network during filtration. These properties include the flow resistance and the stress-strain relation of the network. New information on these important topics can indeed be obtained by utilizing also the momentum Equations (3)

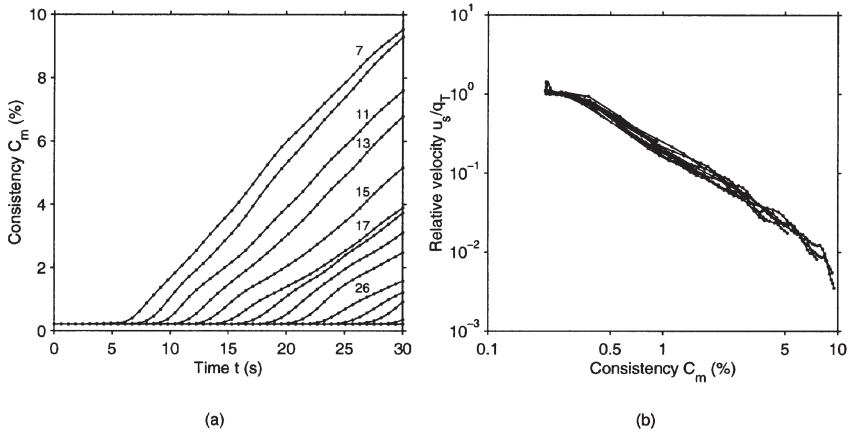

Figure 3 **a)** Mass consistency C_m of dry fibres as a function of time along a subset of pathlines shown in Fig. 2. Selected curves are labelled by the initial z-coordinate (distance from the wire) of the corresponding pathline. **b)** Relative velocity $\tilde{u}_s/q_T$ as a function of consistency along the same pathlines.

and (4) in analysing the experimental data. In order to accomplish such an analysis the interaction term D that appears in the momentum equations and the volume fractions ϕ_a for the two phases must be known. In what follows we assume that the interaction (momentum transfer) between phases is given by a Darcy-type drag force density of the form [17]

$$D = -\frac{\mu}{k}(\tilde{u}_f - \tilde{u}_s), \tag{10}$$

where μ is the dynamic viscosity of the fluid phase and k is the permeability coefficient of the fibre network that depends on volume fractions. In this study we shall assume that permeability is given by the Kozeny–Carman equation which, with the definitions and conventions defined above, can be written as

$$k = k_S \frac{1 - \phi_s}{\phi_s^{\,2}}, \tag{11}$$

where k_s is the specific permeability constant. (In a more usual form of the Kozeny–Carman equation $(1 - \phi_s)^3$ instead of $1 - \phi_s$ appears in the nominator in Equation (11). The difference arises from the slightly different conventions and definitions used in writing the momentum Equations (3) and (4), and the Darcy's equation that defines the permeability coefficient in the conventional formulation of flow in porous medium [17].)

The volume fraction of the solid phase may be related to the mass consistency of dry fibres approximately by

$$\phi_s \cong \frac{C_m}{100}\left(\frac{\tilde{\rho}_f}{\tilde{\rho}_c} + MR_b\right), \tag{12}$$

where $\tilde{\rho}_c$ is the density of dry fibre material and MR_b is the ratio of the bound water mass to the dry fibre mass. In what follows we use the values $\tilde{\rho}_f = 1000$ kg/m^3, $\tilde{\rho}_c = 1500$ kg/m^3 and $MR_b = 1.0$. The density of the solid phase (wet fibres) is then given by

$$\tilde{\rho}_s = \tilde{\rho}_c \frac{(1 + MR_b)}{(1 + \tilde{\rho}_c MR_b/\tilde{\rho}_w)} \approx 1200 \frac{\text{kg}}{\text{m}^3}, \tag{13}$$

With these extra assumptions, we can solve the volume fractions of both phases in the entire flow region. Since the total flux q_T is independently

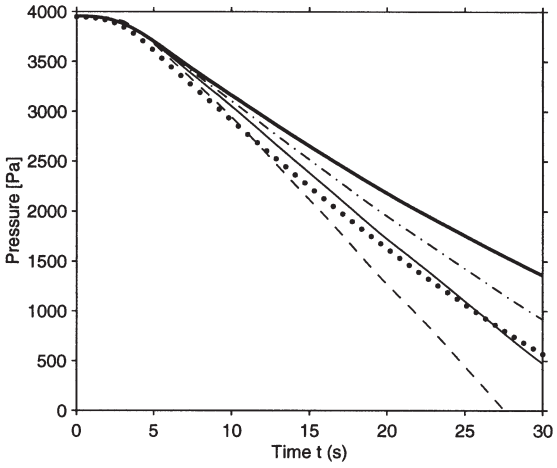

Figure 4 Measured and calculated pressures at $z = 0$. Thick solid line is the calculated total pressure $p_T(t,0)$. Thin lines show the calculated fluid pressure $\tilde{p}_f(t,0)$ for various values of the specific permeability constant. Thin solid line is for $k_S = 1.2 \cdot 10^{-12}$ m$^2 \equiv k_{S0}$, dashed line is for $k_s = \frac{1}{2} k_{S0}$ and dot-dashed line is for $k_s = 2k_{S0}$. Solid symbols are the corresponding measured values of fluid pressure.

measured, we can thus solve fluid velocity $\tilde{u}_f(t,z)$ using Equation (6). Furthermore, at any constant value of time t we can integrate Equations (3) and (4) with respect to spatial coordinate z downwards from the instantaneous measured location of the free surface where all the pressures vanish. We thereby find the fluid pressure field $\tilde{p}_f(t,z)$, the solid pressure $p_s(t,z)$ and, as a sum of these two, the total pressure $p_T(t,z)$. Figure 4 shows the measured and calculated fluid pressure and the calculated total pressure at $z = 0$ (at the wire). A rough overall agreement with the measured fluid pressure is achieved using the value $k_s = 1.2 \cdot 10^{-12}$ m^2 for the specific permeability constant. Notice however that this value and the calculated behaviour of fluid pressure depend on the selected form of the permeability function $k(\phi_s)/k_S$, here given by Kozeny–Carman law, Equation (11). A closer agreement with the measured fluid pressure behaviour might be achieved by a more careful choice of the permeability function. A detailed study of this topic was left outside of the present work.

The values of the solid pressure p_s calculated using Equation (4) depend on various assumptions made above and especially on the value of constant k_S. It appears, however, that for realistic values of that constant, the gravity term

on the right side of Equation (4) is negligible as compared to the drag term D given by Equations (10) and (11). Since the velocities $\tilde{u}_s$ and $\tilde{u}_f$ are fixed experimentally, it follows that the calculated solid pressure is approximately proportional to μ/k. Based on this order of magnitude analysis we ignore the gravity term (buoyance) in Equation (4) and convert it in dimensionless form by defining the dimensionless variables $z^* = z/h_0$, $u_a^* = \tilde{u}_a/U$ and $p_s^* = p_s/\Pi$. Here h_0 is the initial height of the fluid column above the wire, U is a velocity scale appropriate for the experiment, $\Pi = \mu h_0 U/k_0$ is the pressure scale and $k_0 = k(\phi_{s0})$ is the permeability coefficient at the initial state of suspension with solid volume fraction ϕ_{s0}. The dimensionless solid pressure thus fulfils the approximate equation

$$\phi_f \frac{\partial}{\partial z^*} p_s^* \approx \frac{k_0}{k}(u_f^* - u_s^*). \tag{14}$$

Solved from Equation (14), p_s^* does not depend on the value of constant k_S. It does however depend on the dimensionless permeability function $k(\phi_s)/k_S$. It also depends weakly on other assumptions and choices made above, such as the value of the bound water moisture ratio MR_b. Taking $\mu = 0.001$ kg/ms, $h_0 = 0.4$ m, $k_S = 1.2 \cdot 10^{-12}$ m^2, whereby $k_0 \approx 9.4 \cdot 10^{-8}$ m^2, and $U = q_T^{\max} \approx 0.01$ m/s, the absolute scale for the solid pressure is given by $\Pi \approx 50$ Pa.

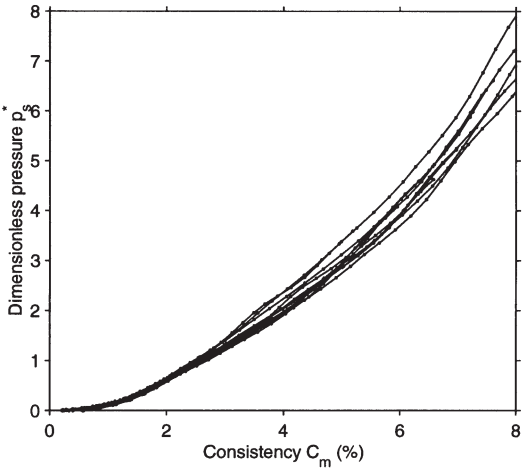

Figure 5 Dimensionless solid pressure (the vertical normal stress of the fibre network) as a function of consistency along a set of solid pathlines.

Figure 5 shows the calculated dimensionless solid pressure as a function of consistency along a set of pathlines. Again, the data for all the pathlines collapse approximately on the same line indicating similar stress behaviour for all layers of the fibre network. The particular result shown in Figure 5 is well fitted by a power law of the form $p_s^* = 0.19 \cdot (C_m - C_{m0})^{1.75}$. The data can thus be considered to represent a valid material property, namely the experimental stress-strain relation of the fibre network during filtration.

5. CONCLUSIONS

We have introduced a novel method for a local measurement of slow filtration of liquid-fibre suspension in a gravity driven laboratory filtration device. The method is in a large part based on pulsed ultrasound-Doppler anemometry that is used to measure the local time-dependent velocity field of the fibre phase in a region including the filtrated fibre layer on top of a wire. Simultaneously, the total flux of the suspension is measured using ultrasound surface detector, and fluid pressure at the bottom of the filtrating layer is detected using a sensor placed underneath the wire. The measurement is non-disturbing and its resolution with respect to position, time and velocity is sufficient such that the dynamics of the filtration process can be monitored in a great detail. The analysis of the data utilizes general equations of one dimensional time dependent two-phase flow whereby the relevant flow quantities such as velocities and consistencies can be obtained separately for both phases as a function of time and vertical position. Moreover, through such an analysis it is possible to obtain the local flow resistance, fluid pressure and normal stress (solid pressure) of the fibre network. Such an experimental information on the material properties of the consolidating fibre network is invaluable in order to gain better understanding on various complicated processes of paper-making, forming in particular.

ACKNOWLEDGEMENT

This work was partially funded by the National Technology Agency of Finland.

REFERENCES

1. Norman, Bo, "On the mechanism of dewatering in the twin-wire and press sections", *Nordic Pulp and Paper Res. J.*, **2**(3): 39 (1987).
2. Farnood, R.R., Loewen S.R., and Dodson, C.T.J., "Forming and Formation of Paper", *Products of Papermaking*, Transactions of the tenth fundamental research symposium, Oxford, Sept. C.F. Baker (ed.), Pira International, Leatherhead, p. 183 (1993).
3. Meyer, H., "Hydrodynamics of the Sheet-Forming Process", *Tappi J.*, **54**(9): 1426 (1971).
4. Lindstrom, T., "Some fundamental chemical aspects of paper forming", *Fundamentals of Papermaking*, Vol. 1, C.F. Baker, (ed.), Mechanical Engineering Pub, pp. 311 – 412, London (1989).
5. Gess, J.M., "A Mechanism for the formation of paper from a hetrogeneous fiber-water mix", *Materials Interactions Relevant to the Pulp, Paper and Wood Industries*, D.F. Caulfield, J.D. Passaretti and S.F. Sobczynski (eds.), Materials Research Society symposium proceedings, Vol 197, Materials Research Society, Pittsburgh, Pennsylvania, pp. 269–272 (1990).
6. Wildfong, V.J., Genco, J.M., Shands, J.A. and Bousfield, D.W., "Filtration Mechanics of Sheet Forming. Part I: Apparatus for Determination of Constant-Pressure Filtration Resistance", *J. Pulp Paper Sci.*, **26**(7): 250 (2000).
7. Wildfong, V.J., Genco, J.M., Shands, J.A. and Bousfield, D.W., "Filtration Mechanics of Sheet Forming. Part II: Influence of Fine Material and Compression", *J. Pulp Paper Sci.*, **26**(8): 280 (2000).
8. Ingmansson, W.L. and Andrews, B.D., "High Velocity Water Flow Through Fibre Mats", *Tappi J*., **46**(3): 150 (1963).
9. Mantar, E., Co, A. and Genco, J.M., "Drainage characteristics of pulp slurries under dynamic conditions", *J. Pulp Paper Sci.*, **21**(2): J44 (1995).
10. Soo, S.L., *Multiphase Fluid Dynamics*, Science Press, Beijing (1990).
11. Hwang, G.-J., *Modeling two-phase flows of a fluid and solid mixture*, Clarkson University, Ph.D. Thesis (1989).
12. Hwang, G.J. and Shen, H.H., "Modeling the solid phase stress in a fluid-solid mixture", *Int. J. Multiphase Flow*, **15**: 257 (1989).
13. Kataja, M., Kirmanen, J. and Timonen, J., "Hydrostatic and structural pressure in compressed paper webs and press felts", *Nordic Pulp and Paper Res. J.*, **3**: 162 (1995).
14. Kytömaa, H., Kataja, M. and Timonen, J., "On the effect of pore pressure on the isotropic behavior of saturated porous media", *J. Appl Phys.*, **81**(1) (1997).
15. Terzaghi, K., *From theory to practise in soil mechanics*, John Wiley, NY (1960).
16. Kerekes, R.J. and Schell, C.J., "Characterization of Fibre Flocculation Regimes by a Crowding Factor", *J. Pulp Paper Sci.*, **18**(1): J32 (1992).
17. Scheidegger, E.A., *The Physics of Flow Through Porous Media*, MacMillan Co., New York (1974).

Transcription of Discussion

APPLICATION OF ULTRASOUND ANEMOMETRY FOR MEASURING FILTRATION OF FIBRE SUSPENSION

Markku Kataja[1,2] *and Pekka Hirsilä*[2]

[1]University of Jyväskylä, Department of Physics
[2]VTT Energy

Editor's note: this data was shown as part of the discussion and is shown here for completeness as some of this information was mentioned at the time of the discussion and questions.

PRELIMINARY RESULTS FROM APPLICATION OF ULTRASOUND ANEMOMETRY FOR MEASURING FILTRATION OF FIBRE SUSPENSION

Markku Kataja[1] *and Pekka Hirsilä*[2]

[1]University of Jyväskylä, Department of Physics,
P.O. Box 35, FIN-40351 Jyväskylä, Finland
[2]Present address: Metso Paper Inc., P.O. Box 587,
FIN-40101 Jyväskylä, Finland

ABSTRACT

In this research note we report some preliminary results, not included in the original paper presented in these proceedings, from measuring the properties of consolidating fibre network during filtration of liquid-fibre suspension. The measurement was done in a laboratory hand-sheet mould using a novel method based on pulsed ultrasound Doppler anemometry. The new results presented here include comparison of various permeability correlations found in the literature and of the stress-strain properties of consolidating network for softwood and hardwood fibres.

1 INTRODUCTION

In these proceedings we introduced a novel method for measuring the properties of consolidating wood fibre network during gravity-driven one-dimensional filtration of liquid-fibre suspension in a laboratory hand-sheet mould [1]. The method was based on pulsed ultrasound-Doppler anemometry. The details of the device and of the techniques for data analysis were presented in ref. [1] and will not be repeated here.

The essence of the experimental method is that the one-dimensional (vertical) velocity field $v(t,z)$ of fibres, and the velocity (total flux) $q_T(t)$ of the surface of fluid column in the mould are measured with high resolution using pulsed ultrasound-Doppler anemometer and a separate ultrasound surface detector, respectively. Here t is time and z is the vertical distance from the screen on which filtration takes place. Using the continuity equations of the fluid phase and of the solid phase (wet fibres), the volume fraction of the two phases and the velocity field of also fluid phase can be computed as a function of t and z. Furthermore, integrating the two momentum equations, we can calculate the total pressure $p_T(t,z)$, the fluid pressure $p_f(t,z)$ and the solid pressure $p_s(t,z)$. That, however, requires that the permeability k of fibre network is given as a function of solid volume fraction ϕ_s. In other words, the value of fluid pressure and solid pressure thus obtained depends on the choise of the permeability function $k = k(\phi_s)$, which is unknown *a priori*. On the other hand, the fluid pressure at screen ($z = 0$) is also directly measured during the filtration process. This allows us to study the combatibility of various functional forms of permeability by comparing the measured and the calculated values of fluid pressure at $z = 0$.

Here we have studied five different permeability functions found in the

literature. These include the relation by Kozeny and Carman [2], by Happel [3,5], by Kuwabara [4,5], by Jackson and James [5] and by Koponen et al [6]. These functions are as follows

$$\frac{k}{k_0} = \frac{(1-\phi_s)}{\phi_s^2} \quad ; \text{Kozeny-Carman ,} \quad [2]$$

$$\frac{k}{a^2} = \frac{1}{8\phi_s(1-\phi_s)^2}\left(-\ln\phi_s + \frac{\phi_s^2-1}{\phi_s^2+1}\right) \quad ; \text{Happel (1959),} \quad [3,5]$$

$$\frac{k}{a^2} = \frac{1}{8\phi_s(1-\phi_s)^2}\left(-\ln\phi_s - \frac{3}{2} + 2\phi_s\right) \quad ; \text{Kuwabara (1959),} \quad [4,5]$$

$$\frac{k}{a^2} = \frac{3}{20\phi_s(1-\phi_s)^2}(-\ln\phi_s - 0.931) \quad ; \text{Jackson \& James (1986),} \quad [5]$$

$$\frac{k}{a^2} = 5.55\left((1-\phi_s)^2(e^{10.1\phi_s}-1)\right)^{-1} \quad ; \text{Koponen et al. (1997).} \quad [6]$$

Here, k_0 is the specific permeability (in Kozeny-Carman relation) and a is the radius of fibres.

The Kozeny-Carman relation is one of the most widely used permeability correlations for porous media. Even though it is well known that Kozeny-Carman relation may not be most suitable for fibrous porous materials with high porosity, we include it here since it is nevertheless frequently used also in analysis of fluid flow in paper, press fabrics etc. The rest of the correlations listed above are specifically derived for fibrous porous materials. The formulas by Happel, by Kuwabara and by Jackson and James (see ref. [5] and references therein) are analytic results applicable for relatively high porosities. The result by Koponen et al [6] is an interpolation formula obtained from direct numerical simulations using the lattice-Boltzmann numerical method. The shapes of these five permeability correlations are shown in Figure 1.

In Figure 2 we show the measured fluid pressure at screen (at $z = 0$) as a function of time for softwood fibres. Also shown are the total pressure and the fluid pressure at $z = 0$ as calculated utilizing the velocity data and the momentum equations with three different permeability functions. In each case, the value of the unknown parameter (k_0 or a) was found by fitting the calculated function $p_f(t, z = 0)$ with the measured pressure data. As shown in Figure 2, all of the three permeability functions give a reasonably good fit to the measured data for softwood fibres. (The results corresponding to permeability functions given by Happel and by Jackson and James are not shown in the figure. These results are very close to those obtained by using the correlation

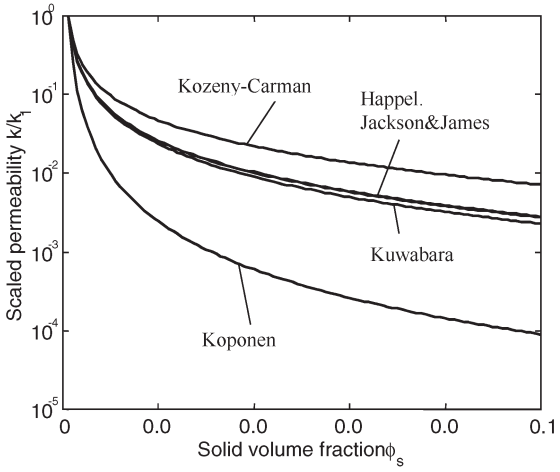

Figure 1 The permeability correlations tested in this work as a function of solid volume fraction ϕ_s. The curves are arbitrarily scaled to unity at $\phi_s = 0.001$ to allow for comparison of the functional shapes.

Table 1 Fitted values of the free parameters and the fit residual for various permeability functions (unbeaten softwood fibres, $MR_b = 1.5$, see ref. [1], Equation (12)).

Perm. model	**Fitted values**	**Fit residual**
	k_0 (m^2)	
Kozeny-Carman	$1.4 \cdot 10^{-12}$	$3.8 \cdot 10^{-4}$
	$2a$ (μm)	
Happel	18.1	$1.8 \cdot 10^{-4}$
Kuwabara	20.4	$1.6 \cdot 10^{-4}$
Jackson and James	16.3	$1.8 \cdot 10^{-4}$
Koponen et al.	32.9	$2.0 \cdot 10^{-4}$

by Kuwabara.) In Table 1 given are the corresponding fitted values of the unknown parameters that appear in each permeability function. For the formulas especially derived for fibrous structures, the free parameter is the fibre radius a. As shown by the table, the fitted diameter is of a correct order of magnitude for all cases (for pine fibres $2a \approx 30$ μm). The most accurate result

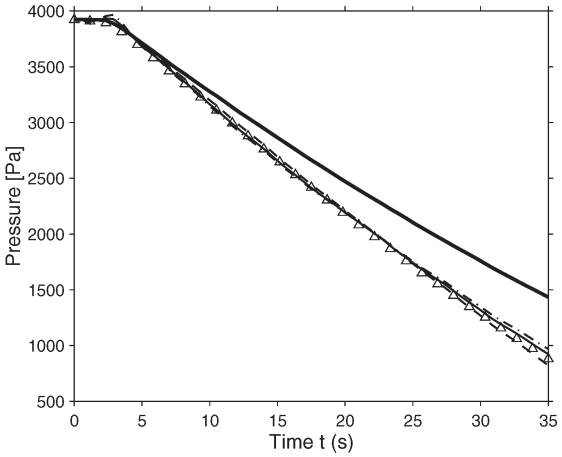

Figure 2 The measured and the calculated pressure values at screen ($z = 0$) during filtration for unbeaten softwood fibres. The solid thick line is the calculated total pressure. The measured values of fluid pressure are given by open triangles. Also shown are the fluid pressure values calculated using the permeability model by Kozeny-Carman (dashed line), by Kuwabara (thin solid line) and by Koponen et al. (dash-dotted line).

in this respect is given by the result by Koponen et al. Notice however, that the analytical and numerical results used here, excluding Kozeny-Carman, are obtained for smooth regular fibres, while wood fibres are irregular in shape and have fine structured surface. Consequently, real wood fibres have higher specific surface area. We may thus expect the effective diameter of fibres, as calculated from the measured value of permeability, to be less than the geometrical mean radius of fibres.

Also given in the Table 1 are fit residuals for each permeability function. A small value of the residual indicates good agreement between measured and calculated pressure values. For softwood fibres the best fit is achieved by using the permeability function of Kuwabara while the worst fit is given by the Kozeny-Carman result.

In Figure 3 and in the Table 2, we show the same data as in Figure 2 and Table 1, but for hardwood fibres (birch). Also in this case the best agreement with measured data is obtained by the Kuwabara result, while the result corresponding to Kozeny-Carman formula is clearly off the measured data. The fitted values of fibre diameter are again of a correct order of magnitude (for birch fibres $2a \sim 20$ μm).

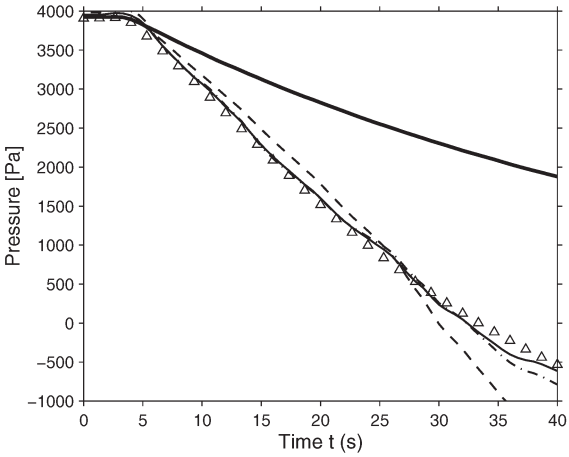

Figure 3 Same as Figure 2, but for unbeaten hardwood fibres.

Table 2 Same as Table 1, but for unbeaten hardwood fibres ($MR_b = 1.0$, see ref. [1], Equation (12)).

Perm. model	**Fitted values**	**Fit residual**
	k_0 (m^2)	
Kozeny-Carman	$0.75 \cdot 10^{-12}$	$72 \cdot 10^{-4}$
	$2a$ (μm)	
Happel	10.5	$13 \cdot 10^{-4}$
Kuwabara	12.0	$9.4 \cdot 10^{-4}$
Jackson and James	9.7	$44 \cdot 10^{-4}$
Koponen et al.	18.1	$21 \cdot 10^{-4}$

Figure 4 shows the calculated solid pressure p_s as a function of solid mass consistency C_m along a number of solid pathlines (in t-z -plane, see Figure 2 in ref. [1]) for softwood fibres and for hardwood fibres. The most remarkable feature of this result is that the data points for all pathlines fall quite closely on a single curve in C_m-p_s -plane (for softwood and for hardwood fibres separately). This indicates, that the result indeed reflects a true material property, namely the stress-strain behaviour of the consolidating fibre network during filtration! As expected, the network formed by birch fibres appears

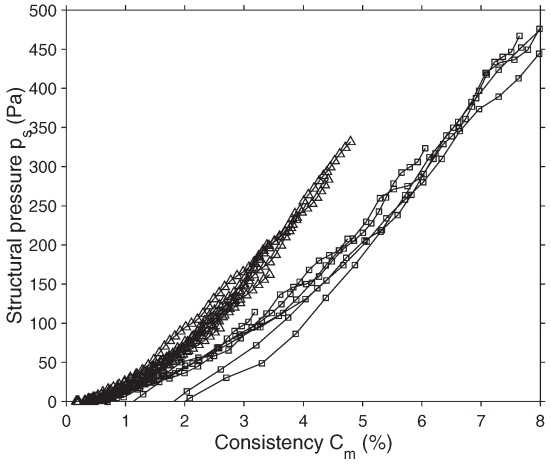

Figure 4 Solid pressure as a function of consistency along pathlines for unbeaten softwood fibres (triangles) for unbeaten hardwood fibres (squares).

softer than that formed by pine fibres. For the data shown in Figure 4, the initial consistency was 0.2% for softwood fibres and 0.4% for hardwood fibres. Both consistencies correspond to a growding number of approximately 15 [7]. Notice, that the measured stress-strain correlation depends on the permeability function used in data analysis. Here, the formula by Kuwabara was used.

In addition to the continuous consolidation discussed above, the device can be used to study more complicated filtration processes. For example, by interrupting the filtration for a certain time, one can extract information on relaxation behaviour and on the intricate rheological properties of fibre structure, such as viscoelasticity, plasticity etc. Figure 5 shows the pressures measured at $z = 0$ in such an experiment for softwood fibres. Here, filtration is interrupted by closing the air valve for a few seconds in the middle of the experiment. This causes the total pressure to level off and the fluid pressure on screen surface to increase and approach the total pressure from below as the flow ceases.

Figure 6 shows the stress-strain history of fibres along two solid pathlines with different initial position during the process. The curves first follow a common path similar to those shown in Figure 4 for continuous consolidation. After the flow is interrupted, fibre network undergoes relaxation which is indicated by a rapid decrease of solid pressure towards zero associated with a slight decrease of also consistency as the fibre network expands. Obviously,

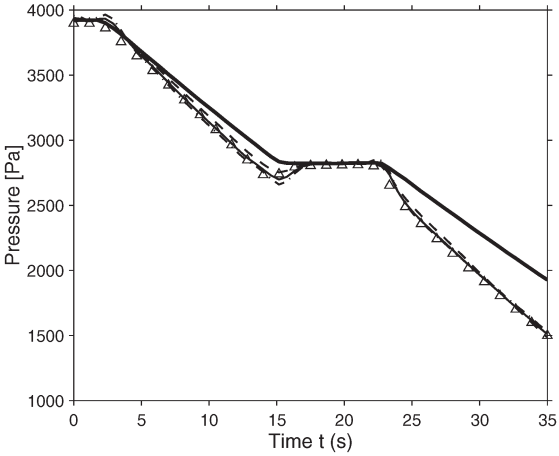

Figure 5 As Figure 2, but for interrupted filtration experiment.

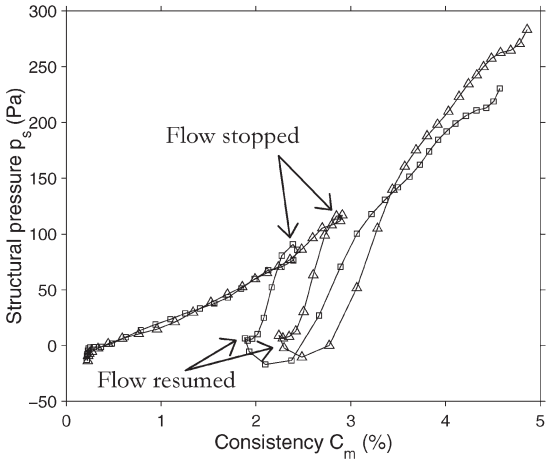

Figure 6 Stress-strain behaviour of softwood fibres along two solid pathlines. The initial position of the pathlines is $z_0 = 55$ mm (triangles) and $z_0 = 80$ mm (squares).

the behaviour of the network at this stage is highly non-elastic. As the flow is resumed, the stress-strain curves again approach the curve of continuous consolidation. The time required to approach the original curve gives a rough estimate of the magnitude of the time constant associated to viscoelastic behaviour of the network. (The time interval between the data points indicated by solid symbols on the curve is 0.58 s.) A more detailed analysis of the stress-strain behaviour of the consolidating fibre network is left in a future work.

2. CONCLUSIONS

Filtration measurement based on the use of pulsed ultrasound Doppler anemometry facilitates a very detailed experimental study of slow one-dimensional filtration of fibre suspensions. Essential material properties, such as the permeability to fluid flow and the stress-strain behaviour of the consolidating fibre network can be studied by utilizing the general two-phase flow equations in the data analysis. The method is presently limited to a relatively low filtration speed (a few cm/s) and to pure fibre suspensions, with no fillers or fines and with a narrow distribution of fibre lengths.

A clear and plausible difference in the flow resistance and stress-strain properties was observed for unbeaten softwood and hardwood fibres. Of the various possibilities tested in this preliminary study, the best compatibility of measured data was obtained using the permeability correlation by Kuwabara.

REFERENCES

1. M. Kataja and P. Hirsilä, "Application of ultrasound anemometry for measuring filtration of fibre suspension", *The Science of Papermaking*, Transactions of the 12th fundamental research symposium, Vol. 1, C. F. Baker (ed.), Oxford, September 2001, The Pulp and Paper Fundamental Research Society, UK 2001, pp. 591–604.
2. E. A. Scheidegger, *The Physics of Flow Through Porous Media*, MacMillan Co., New York 1974.
3. J. Happel, "Viscous flow relative to Arrays of Cylinders", *AIChE J*., **5**, 174 (1959).
4. S. Kuwabara, "The Forces Experienced by Randomly Distributed Parallel Circular Cylinders or Spheres in a Viscous Flow at Small Reynolds Numbers", *J. Phys. Soc. Japan*, **14**, 527 (1959).
5. G. W. Jackson and D. F. James, "The permeability of fibrous porous media", *Can. J. Chem. Eng*., **64**, 364 (1986).
6. A. Koponen, D. Kandhai, E. Hellén, M. Alava, A. Hoekstra, M. Kataja, K.

Niskanen, P. Sloot and J. Timonen, "Permeability of Three-Dimensional Random Fiber Webs", *Phys. Rev. Lett*., **80**, 716 (1998)
7. R. J. Kerekes and C. J. Schell, "Characterization of Fibre Flocculation Regimes by a Crowding Factor", *J. Pulp Paper Sci*., **18**(1), J32 (1992).

Jean-Claude Roux EFPG

In your experimentation you show the movement of the free surface versus the time, and I would like to know if you have obtained results with a slope for expressing the decreasing of the free surface rather than a horizontal slope at the beginning of time?

Markku Kataja

Yes, I think I showed that data already (Figure 2). The slope is the velocity, the total flux.

Jean-Claude Roux

It seems to me that in Figure 2 of your paper where you mention the different curves, the immediate curve has horizontal slope which surprised me (referring to slide 19 (Figure 4)). At the beginning your curve has a horizontal slope and I was wondering if you obtain these results?

Markku Kataja

It is horizontal because the valve is closed at this point, there is no flow! In this experiment I first trigger data acquisition and then after a few seconds, I gradually open the valve and start the flow, slowly in order to reduce inertial effects.

Jean-Claude Roux

I am serious if I say that it is because I believe that the inertial force can have some importance at this point, and the acceleration also can have importance. In the initial equations if we remove the inertial terms and make some discrepancy or some error I can say that you can have some differences at the beginning, because this is a difficult region we are working on this.

Markku Kataja

I am not sure whether this bump in the filled curves near the point where the flow is started comes from inertial terms. It may also come from smoothing of data. Anyway at the point where I open the valve there is a minor inertial effect which I ignore, but the effect disappears very rapidly.

Jean-Claude Roux

I agree with all the results but at the beginning there is great difficulty in studying this problem.

Hannu Paulapuro Helsinki University of Technology

This is a very important and interesting paper. In a way you tried to classify the different types of fibrous materials and their behaviour in an invariable way, which we need when we look at these phenomena. My question is, could you include a pulsating effect in your drainage measurement?

Markku Kataja

We haven't done anything like that. It could probably be done, but only at a relatively slow rate.

Hannu Paulapuro

I wondered if this kind of measuring device could be mounted on equipment like a moving belt former, as a pulsating de-watering as well as a vacuum application.

Markku Kataja

In principle yes, if it could be done in an airless environment. Another difficulty is that with this technique we can only basically measure one component of velocity so we cannot at the moment, measure shear fields of two dimensional flows. I do not know whether that kind of measurement is possible.

John Daicic Institute for Surface Chemistry, Stockholm

Those equations that you showed for permeability at the end i.e. Koseny-

Discussion

Carman equation and all the others do any of them take into account that the sediment should be compressible?

Markku Kataja

The sediment is certainly compressible and that effect is fully accounted for in this analysis.

John Daicic

Do those forms for the permeability account for compressibility i.e. the fact that the sediment is compressing during the sedimentation in the pressure filtration experiment.

Markku Kataja

Yes, it is compressing.

Bill Sampson Department of Paper Science, UMIST

I think the point is that you have the variable for solidity in your equations, Kozeny-Carman and others, and you have shown that you have a solidity profile for the forming mat, so how do you incorporate that variability at the forming mat?

Markku Kataja

I applied the equation locally. I refer to Equations 1–4, 10 and 11 in our paper.

John Daicic

Just one small point, you said that you couldn't have fines or flocs (changed to fillers) in your suspension but the reason that I said flocs was because isn't it the case that, even though you only have fibres you have effectively particles of different sizes falling with different velocities because of the fact that you have flocs there, so you have a distribution of particle sizes effectively.

Markku Kataja

Yes there is a distribution of velocities even in this case of a narrow particle size distribution. That is why I am using four ultrasonic transducers to give

some special averaging already in the measurement stage. The transducers are arranged under the wire such that they measure some quite wide transverse area of the suspension above the wire. In addition to that, some further filtering of data is needed in order to reduce the effects of velocity fluctuations that indeed are present in the original measured signal. Part of that fluctuation is simply 'device noise' irrelevant in the measuring method, and part of that is actual velocity variations that arise due to flocculated structure of fibre network.